

# X-Ray Scattering at Lanthanide $M_5$ Resonances: Application to Magnetic Depth Profiling

H. Ott,<sup>(1,†)</sup> C. Schüßler-Langeheine,<sup>(1,2)</sup> E. Schierle,<sup>(1)</sup> A. Yu.  
Grigoriev,<sup>(1,††)</sup> V. Leiner,<sup>(3)</sup> H. Zabel,<sup>(3)</sup> G. Kaindl,<sup>(1)</sup> and E. Weschke<sup>(1,\*)</sup>

<sup>(1)</sup> *Institut für Experimentalphysik, Freie Universität Berlin, D-14195 Berlin-Dahlem, Germany*

<sup>(2)</sup> *II. Physikalisches Institut, Universität zu Köln, D-50937 Köln, Germany and*

<sup>(3)</sup> *Institut für Experimentalphysik/Festkörperphysik,*

*Ruhr-Universität Bochum, D-44780 Bochum, Germany*

(Dated: November 20, 2018)

Quantitative analyses of x-ray scattering from thin films of Ho and Dy metal at the  $M_5$  resonances result in values of the optical constants and the magnetic scattering lengths  $f_m$ , with  $f_m$  as large as  $200r_0$ . The observation of first- and second-order magnetic satellites allows to separate  $f_m$  into circular and linear dichroic contributions. This high magnetic sensitivity, in conjunction with the tunable x-ray probing depth across the resonance can be applied to monitor depth profiles of complex magnetic structures, as e.g. of helical antiferromagnetic domains in a Dy metal film.

PACS numbers: 61.10.Eq,75.70.Ak,75.25.+z

Magnetism in thin films, nanostructures, and other complex materials is currently a field of considerable interest, where diffraction and scattering methods can provide detailed insight into spin structures and magnetic correlations. While magnetic neutron diffraction had long been the method of choice, resonant magnetic x-ray diffraction using synchrotron radiation [1] has emerged as a complementary technique. Tuning the photon energy to an electronic core excitation leads to an element-specific enhancement of magnetic scattering [2, 3, 4, 5, 6, 7] that is particularly strong at the  $L_{2,3}$  resonances of the  $3d$  transition elements and the  $M_{4,5}$  resonances of lanthanides and actinides. Quite early, Hannon *et al.* predicted that at the  $M_{4,5}$  resonances the magnetic contribution  $f_m$  to the scattering length  $f$  should be of the same order of magnitude as the contribution of charge scattering, with values of  $f_m$  up to  $100r_0$  ( $r_0 =$  classical electron radius) [3]. This agrees with the huge enhancement of magnetic scattering by a factor of  $\approx 10^7$  at the  $M_4$  resonance of uranium [4], leading to sizeable intensities along purely magnetic crystal truncation rods of antiferromagnets, and permitting the study of surface magnetism of  $\text{UO}_2$  [8]. The magnetic sensitivity at resonance is accompanied by strong x-ray absorption (XA), a fact that usually renders a quantitative determination of  $f_m$  from magnetic superstructure peaks difficult [9]. When used properly, however, the strong XA can be exploited to vary the probing depth of magnetic x-ray scattering.

In this Letter, we report on soft x-ray scattering from lanthanide-metal films, providing a quantitative characterization of magnetic scattering at the  $M_5$  resonances, including a separation of  $f_m$  into circular and linear dichroic components and a determination of the resonant index of refraction,  $n = 1 - \delta + i\beta$ . With quantitative values for  $\beta$  in the resonance region, the x-ray probing depth can be tuned in a controlled way, while retaining

high magnetic sensitivity. The probing depth can thus be varied independently of the scattering vector, providing a tool for depth-resolved characterization of complex magnetic structures, complementary to surface scattering along the crystal truncation rods. As an example, a depth-resolved study of the growth of helical antiferromagnetic (AFM) domains across a magnetic phase transition in Dy metal is presented.

The helical AFM structures in Ho and Dy metal are well suited for resonant magnetic soft x-ray studies, since the magnetic periods match the x-ray wavelengths at the respective  $M_5$  resonance. In Ho metal this helical AFM structure persists in films down to 10 monolayers (ML) [10], a thickness range where absorption effects are reduced, simplifying a quantitative determination of  $f_m$ . Soft x-ray studies were carried out in an ultra-high-vacuum (UHV) ( $\Theta/2\Theta$ ) diffractometer on *in-situ* grown lanthanide-metal films on W(110) [10] and on Y/Ho/Y trilayer samples prepared *ex situ* by molecular-beam epitaxy (MBE) on *a*-plane sapphire [11]. For all samples, the *c* axis was perpendicular to the film surface.  $M_5$  resonance data were taken at beamline U49/1 of the Berliner Elektronenspeicherring für Synchrotronstrahlung (BESSY) with linearly polarized x rays ( $\pi$  polarization). Resonant Dy  $L_3$  data (at  $\approx 8$  keV) were recorded at beamline ID 10 A of the European Synchrotron Radiation Facility (ESRF) in Grenoble.

The resonant enhancement of magnetic x-ray scattering at the  $M_5$  resonance and the concomitant strong absorption are illustrated in Fig. 1(a), which displays specular reflectivity curves from 110 ML Ho on W(110) at 40 K, well below the bulk Néel temperature ( $T_N = 131.2$  K). Far below resonance ( $h\nu = 900$  eV), the reflectivity is dominated by intensity oscillations (Kiessig fringes) caused by interference of x rays scattered from the surface with those scattered from the Ho/W interface [12]. At  $h\nu = 1340$  eV, 14 eV below the  $M_5$  reso-

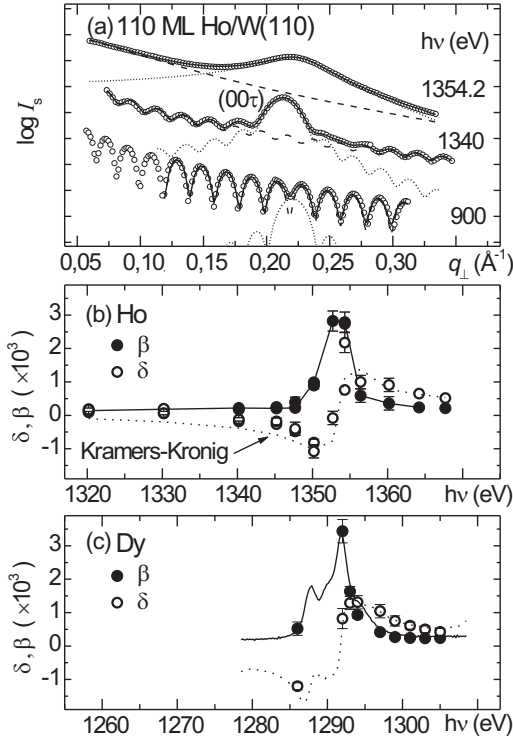


FIG. 1: (a) Specularly reflected intensities ( $I_s$  on a log-scale) from 110 ML Ho/W(110) versus momentum transfer  $q_{\perp}$  (data for different photon energies are vertically offset). The solid lines represent fits with a superposition of magnetic (dotted) and charge (dashed) contributions. Lower panels: optical parameters  $\beta$  (solid symbols) and  $\delta$  (open symbols) of (b) Ho and (c) Dy metal in the  $M_5$  region. The dotted lines represent the Kramers-Kronig transforms of the  $\beta$  values in (b), and  $\beta$  obtained from the scaled XA spectrum (solid line) in panel (c).

nance maximum, the diffraction peak caused by the magnetic superstructure, labeled  $(00\tau)$ , is already clearly visible. At maximum resonance ( $h\nu = 1354.2$  eV), the substantial XA strongly alters the reflectivity curve:  $(00\tau)$  is broadened due to the reduced number of layers that contribute to the magnetic signal [9], and the Kiessig fringes are completely suppressed, since the x rays no longer penetrate to the Ho/W interface.

As a first step towards a determination of  $f_m$ , the resonant optical constants were derived from reflectivity curves by fit analyses using the Parratt formalism [13]. Far from resonance, tabulated values of  $\beta$  and  $\delta$  [14] are reliable and were used to fit the 900-eV data, yielding the structural parameters of the film [15]. The optical constants at a given resonance energy were then obtained from a fit of the respective reflectivity curve with  $\beta$  and  $\delta$  as the only adjustable parameters. The superimposed magnetic peak was described by the structure factor of a helix, taking a mean magnetic roughness and an angle-dependent polarization factor into account [7]. Refraction and absorption corrections to the shape of the magnetic peak were accounted for by a complex scattering

vector.

The resulting  $\beta$  and  $\delta$  values are plotted in Fig. 1(b); they are consistent with a Kramers-Kronig (KK) transform of  $\beta$  that reproduces  $\delta$  rather well. At maximum resonance,  $\beta = (2.8 \pm 0.3) \cdot 10^{-3}$  is obtained, a value that fits well with recent results for Gd and Tb [16], and corresponds to a photon attenuation length of  $1/\mu = \lambda/4\pi\beta \approx 260$  Å, i.e., an effective probing depth of only  $\approx 28$  Å at the magnetic peak position (scattering angle  $\Theta \approx 12.5^\circ$  with respect to the sample surface). Similar data were obtained for Dy as shown in Fig. 1(c). Here, the solid line represents  $\beta$  values obtained from the Dy  $M_5$  XA spectrum, the KK transform of which consistently reproduces the  $\delta$  values obtained from the reflectivity curves.

For a quantitative determination of  $f_m$ , a thin Y/Ho/Y film was used that exhibits a larger  $\tau$  compared to Ho/W(110) [11] and hence a smaller charge-scattering background at  $(00\tau)$ . Figure 2(a) displays the  $M_5$  XA spectrum of Ho with its atomic  $3d^9 4f^{11}$  final-state multiplet that separates into three subspectra with  $\Delta J = 0, \pm 1$  [17, 18]. In the presence of magnetic order, the  $J$  states split into  $M_J$  sublevels, and the transitions are governed by the selection rule  $\Delta M_J = 0, \pm 1$ . In the heavy lanthanides, the transition probabilities for a given  $\Delta J$  are dominated by a *single*  $\Delta M_J$  value, and the subspectra can then be identified approximately by  $\Delta M_J = 0, \mp 1$ , respectively [18]. These dipole transitions determine the resonant scattering length [3, 7]

$$f = (\mathbf{e}' \cdot \mathbf{e}) \cdot f_0 - i(\mathbf{e}' \times \mathbf{e}) \cdot \mathbf{m} \cdot f_m^c + (\mathbf{e}' \cdot \mathbf{m})(\mathbf{e} \cdot \mathbf{m}) \cdot f_m^l, \quad (1)$$

with  $f_0 = a(F_{+1}^1 + F_{-1}^1)$ ,  $f_m^c = a(F_{+1}^1 - F_{-1}^1)$ , and  $f_m^l = a(2F_0^1 - F_{+1}^1 - F_{-1}^1)$ . Here, the  $F_{\Delta M_J}^1$  denote the energy-dependent dipole oscillator strengths with  $\Delta M_J = 0, \pm 1$ , and  $\mathbf{e}$  and  $\mathbf{e}'$  the polarization vectors of incident and scattered x rays, respectively.  $a = (3/4\pi k)$  is a wave-vector dependent factor and  $\mathbf{m}$  is the unit vector in direction of the local magnetic moment.

For Ho, circular ( $f_m^c$ ) and linear ( $f_m^l$ ) dichroic terms in Eq. 1 are readily distinguished, since the corresponding diffraction peaks at  $(00\tau)$  and  $(002\tau)$  are well separated in momentum space (inset in Fig. 2(b)). The resonant  $(00\tau)$  peak at  $2\Theta \approx 25^\circ$  is due to  $f_m^c$  with a polarization factor *linear* in  $\mathbf{m}$ . Characterized by a sinusoidal modulation, the magnetic structure of Ho contains no higher harmonics, and the  $(002\tau)$  peak at  $2\Theta \approx 50^\circ$  is thus solely a resonance effect due to  $f_m^l$  [19]. With a polarization factor *quadratic* in  $\mathbf{m}$ ,  $f_m^l$  gives rise to a resonant peak at  $(002\tau)$ , since  $\mathbf{m}^2$  oscillates with half the magnetic period. The linear dichroic term  $f_m^l$  generally probes elements that preserve time-reversal symmetry [20]; therefore it can be used to study the ordering of quadrupole moments in non-spherical charge densities. In the present case of AFM Ho metal, however, a distinction of quadrupolar and spin linear dichroism is of no significance, since the strong spin-orbit interaction of the atomic-like  $4f$  states couples the arrangement of the quadrupole moments to

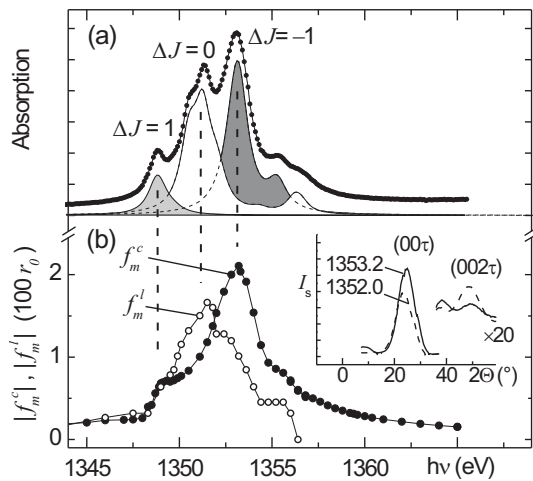


FIG. 2: (a)  $M_5$  XA spectrum of 31 ML Ho/W(110) recorded via sample drain current. The subpeaks represent calculated  $\Delta J = 0, \pm 1$  transitions [17]. (b) Magnetic scattering lengths  $|f_m^c|$  and  $|f_m^l|$ . The inset shows reflectivity curves (on a linear scale) from a 16-ML Ho MBE film, taken at the two given photon energies (in eV).

the spin structure [21]. The  $(00\tau)$  and  $(002\tau)$  can be entirely described by  $f_m^c$  and  $f_m^l$ , respectively, according to the  $\Delta M_J = 0, \pm 1$  transitions from the  $M_J$  sublevels of the helical AFM ground state of Ho.

From the respective integrated intensities,  $|f_m^c|$  and  $|f_m^l|$  were calculated, taking polarization factors [7] and absorption corrections into account ( $\beta$  values from Fig. 1(b)). The resulting  $|f_m^c|$  and  $|f_m^l|$  are plotted in Fig. 2(b), revealing a clear correspondence to the subpeaks in Fig. 2(a):  $|f_m^c|$  peaks at the maxima of the  $\Delta J = \pm 1$  subpeaks, whereas  $|f_m^l|$  peaks at the maximum of the  $\Delta J = 0$  subpeak. Thus, the  $3d^9 4f^{11}$  multiplet of Ho allows to identify the circular and linear dichroic contributions to the scattering length; such a separation is not equally straightforward in case of the actinides [19]. We obtain  $|f_m^c| = 200r_0$  and  $|f_m^l| = 160r_0$  at the respective resonance maxima, i.e. values that are somewhat larger, but of the same order of magnitude as predicted [3].

An application that exploits both the tunable x-ray probing depth and the high magnetic sensitivity across the resonance is the study of depth-dependent inhomogeneous magnetic structures, even in case of chemically homogeneous materials. We demonstrate the potential of the method for the growth of helical AFM domains at the ferromagnetic (FM)/helical-AFM first-order phase transition of Dy metal [22]. As shown in Fig. 3(a) for a 180-ML film of Dy on W(110), this transition exhibits substantial hysteresis. Here, the integrated intensity of  $(002-\tau)$  is displayed [1, 2], recorded at the  $L_3$  resonance of Dy ( $h\nu = 7780$  eV), where all layers of the film contribute about equally to the magnetic signal; the x-ray probing depth of  $\approx 9 \mu\text{m}$  is much larger than the film

thickness of  $\approx 500 \text{ \AA}$ . Due to the weaker magnetic sensitivity at  $L_3$  as compared to  $M_5$ , a polarization analysis was required to separate  $(002-\tau)$  from the charge-scattering background [1, 2]. When cooling to the FM phase (open symbols),  $(002-\tau)$  disappears at  $\approx 70$  K; it reappears when heating, but with a delay of  $\approx 20$  K (solid symbols). Notably, the  $(002-\tau)$  intensity does not recover abruptly, but remains below the cooling-down curve up to  $\approx 140$  K, indicating a temperature-dependent growth of helical AFM domains. This is further characterized by the widths of the magnetic diffraction peaks displayed in Fig. 3(c), both in the direction perpendicular ( $W_{q\perp}$ ) and parallel ( $W_{q\parallel}$ ) to the film plane.  $W_{q\perp}$  was determined both for  $(002-\tau)$  at the  $L_3$  (squares) and for  $(00\tau)$  at the  $M_5$  (circles) resonance. The smaller  $W_{q\parallel}$  was measured only at the  $M_5$  resonance, where sufficient momentum resolution could be achieved. When cooling,  $W_{q\perp}$  remains essentially constant down to  $\approx 70$  K;  $W_{q\perp} \approx 1.2 \times 10^{-2} \text{ \AA}^{-1}$  corresponds to 180 ML of Dy, i.e., the helical AFM structure extends through the whole film. Below  $\approx 70$  K,  $W_{q\perp}$  increases abruptly with the decay of the helical AFM order and – with increasing temperature – exhibits the same hysteresis as the intensity of  $(002-\tau)$ . In contrast,  $W_{q\parallel}$  is essentially constant in the studied temperature range, showing that the helical AFM domains develop in a laterally homogeneous way in the direction perpendicular to the film plane.

For a depth-resolved characterization of domain growth,  $(00\tau)$  was studied at the Dy  $M_5$  resonance.

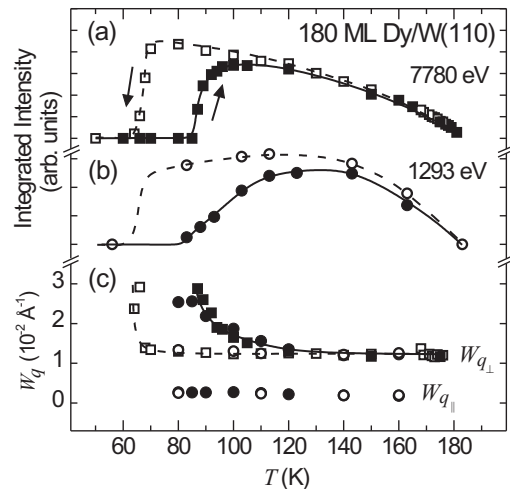


FIG. 3: Magnetic diffraction data characterizing the FM/helical-AFM phase transition in 180-ML Dy/W(110) upon cooling down (open symbols) and warming up (filled symbols); lines serve as guides to the eye. (a) Integrated intensities of  $(002-\tau)$  at the  $L_3$  resonance (7780 eV). (b) Analogous data from  $(00\tau)$  recorded at the  $M_5$  resonance. (c) Widths of magnetic peaks in the direction parallel ( $W_{q\parallel}$ ) and perpendicular ( $W_{q\perp}$ ) to the film plane recorded at 7780 eV (squares) and at 1305 eV (circles).

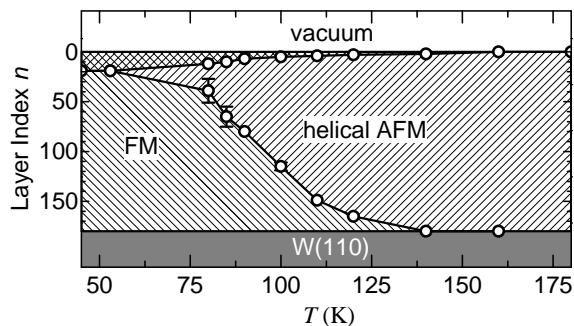


FIG. 4: Temperature-dependent growth of helical AFM domains in 180-ML Dy/W(110) in the direction perpendicular to the film plane. For details, see text.

Fig. 3(b) displays the integrated intensities obtained at  $h\nu = 1293$  eV where the effective x-ray probing depth is only  $\approx 35$  Å. Here, the delayed formation of the helical AFM phase upon heating is more pronounced than at 7780 eV excluding a nucleation of the helical domain in the *topmost* surface layer. Instead, the domain nucleates close to the surface as discussed below. A further detail of the reflectivity curves recorded at highest surface sensitivity (data not shown here) is the occurrence of a magnetic signal at smaller scattering angles in addition to  $(00\tau)$ . This is the signature of a surface AFM structure with a larger mean modulation period in the surface layers of the film that develops when cooling below  $\approx 125$  K and that disappears upon heating above this temperature. Such a structure had previously been reported for a 10-ML thick Ho film [23], and results from the tendency of helical AFM lanthanide films to favor FM order in the surface region [10].

The complete depth profile, shown in Fig. 4, was derived from data recorded with various x-ray probing depths across the Dy  $M_5$  resonance. The  $\beta$  values determined for the same film (Fig. 1(c)) allowed an analysis, where the magnetic scattering amplitude of an individual layer  $n$  at depth  $d_n$  is reduced by  $e^{-\mu d_n / \sin\theta}$  [9]. The consistent analysis of temperature-dependent intensities leads to the following scenario: Upon cooling, the whole film orders helical AFM below  $T_N \approx 179$  K. Below  $\approx 125$  K, the surface AFM structure develops as described above, consistent with the minute increase of  $W_{q\perp}$  by  $\approx 1\%$  in this temperature region. Below  $\approx 70$  K, the film turns FM, except for the topmost  $\approx 19$  layers that retain the surface AFM structure (cross-hatched area). Upon heating, the helical AFM domain nucleates below this surface region and grows with increasing  $T$  towards the two interfaces. When reaching  $\approx 140$  K, it has developed across the whole film.

We point out that the present approach of exploiting the tunable x-ray probing depth across a resonance is not restricted to magnetic signals, and is also applicable

to systems containing 3d transition elements, where at the  $L_{2,3}$  resonances similarly strong absorption has been observed [24]. Such depth-dependent diffraction studies will be particularly interesting with focused x-ray beams providing additionally lateral resolution [25].

Expert support by the staff members of BESSY and the ESRF is gratefully acknowledged, particularly the commitment of G. Grübel. We acknowledge helpful discussions with M. W. Haverkort. The work was financially supported by the BMBF, projects 05KS1KEE/8 and 03ZA6BC2, the Sfb-290 (TPA06) of the DFG, and the Landesministerium NRW für Wissenschaft und Forschung.

- 
- [\*] Corresponding author:  
eugen.weschke@physik.fu-berlin.de
  - [†] present address: II. Physikalisches Institut, Universität zu Köln, D-50937 Köln, Germany
  - [††] present address: Department of Materials Science and Engineering, University of Wisconsin, Madison, WI 53706, U.S.A.
  - [1] D. Gibbs *et al.*, Phys. Rev. Lett. **55**, 234 (1985).
  - [2] D. Gibbs *et al.*, Phys. Rev. Lett. **61**, 1241 (1988).
  - [3] J. P. Hannon *et al.*, Phys. Rev. Lett. **61**, 1245 (1988).
  - [4] E. D. Isaacs *et al.*, Phys. Rev. Lett. **62**, 1671 (1989).
  - [5] J. M. Tonnerre *et al.*, Phys. Rev. Lett. **75**, 740 (1995).
  - [6] M. Sacchi *et al.*, Phys. Rev. Lett. **81**, 1521 (1998).
  - [7] S. W. Lovesey and S. P. Collins, *X-ray Scattering and Absorption by Magnetic Materials*, Clarendon Press, Oxford (1996), p. 180ff.
  - [8] G. M. Watson *et al.*, Phys. Rev. B **61**, 8966 (2000).
  - [9] N. Bernhoeft *et al.*, Phys. Rev. Lett. **81**, 3419 (1998).
  - [10] E. Weschke, *et al.*, Phys. Rev. Lett. **93**, 157204 (2004).
  - [11] V. Leiner, *et al.*, Physica B **283**, 167 (2000).
  - [12] J. Als-Nielsen and D. McMorrow, *Elements of Modern X-Ray Physics*, John Wiley & Sons, New York (2001).
  - [13] L. G. Parratt, Phys. Rev. **95**, 359 (1954).
  - [14] B. L. Henke, E. M. Gullikson, and J. C. Davis, At. Data Nucl. Data Tables **54**, 181 (1993); [http://www-cxro.lbl.gov/optical\\_constants](http://www-cxro.lbl.gov/optical_constants).
  - [15] For the present film, we obtain a thickness of 110 ML  $[(309 \pm 1) \text{ Å}]$ , and a combined surface and interface roughness of  $(1.0 \pm 0.5) \text{ Å}$ .
  - [16] J. E. Prieto *et al.*, Phys. Rev. B **68**, 134453 (2003).
  - [17] J. B. Goedkoop *et al.*, Phys. Rev. B **37**, 2086 (1988).
  - [18] J. Ph. Schillé *et al.*, Phys. Rev. B **48**, 9491 (1988).
  - [19] D. Mannix *et al.*, Phys. Rev. B **62**, 3801 (2000).
  - [20] S. B. Wilkins *et al.*, Phys. Rev. B **70**, 214402 (2004).
  - [21] M. Amara and P. Morin J. Phys.: Condens. Matter **10**, 9875 (1998).
  - [22] M. K. Wilkinson *et al.*, J. Appl. Phys. **32**, 48S (1961).
  - [23] E. Weschke *et al.*, Synchr. Rad. News **295**, 1042 (2002).
  - [24] J. B. Kortright and Sang-Koog Kim, Phys. Rev. B **62**, 12216 (2000).
  - [25] P. G. Evans *et al.*, Science **295**, 1042 (2002).